International Journal of Heat and Fluid Flow 29 (2008) 1154–1163

Contents lists available at ScienceDirect

International Journal of Heat and Fluid Flow

journal homepage: www.elsevier.com/locate/ijhff

Natural convection in a horizontal binary fluid layer bounded by thin porous layers

Z. Alloui [a,*], M. Fekri [a], H. Beji [b], P. Vasseur [a]

[a] Ecole Polytechnique, Université de Montréal, C.P. 6079, Succ. «Centre Ville», Montréal, Québec, Canada H3C 3A7
[b] Laboratoire des Technologies Innovantes, Université Jules Vernes d'Amiens, rue des Facultés le Bailly, 800025 Amiens Cedex, France

ARTICLE INFO

Article history:
Received 6 February 2008
Received in revised form 18 March 2008
Accepted 27 March 2008
Available online 19 May 2008

Keywords:
Natural convection
Fluid layer
Beavers–Joseph slip condition
Double diffusion
Soret

ABSTRACT

This paper reports an analytical and numerical study of natural convection in a horizontal binary fluid layer confined between two horizontal porous walls. The cavity is heated from the bottom by a constant heat flux while the long side walls are impermeable and adiabatic. The Beavers–Joseph slip condition on velocity is applied at the interface between the fluid and porous layers. Both double-diffusive convection and Soret-induced convection are considered. An analytical model, based on the parallel flow approximation, is proposed for the case of a shallow layer. The flow and heat and mass transfer variables are obtained in terms of the governing parameters of the problem. The critical Rayleigh numbers for the onset of supercritical and subcritical convection are predicted for various hydrodynamic boundary conditions. The results for a fluid layer bounded by solid walls and free surfaces emerge from the present analysis as limiting cases. The study is completed by a numerical solution of the full governing equations.

1. Introduction

Rayleigh–Benard convection in a horizontal binary fluid layer has received considerable attention since this phenomenon can be found in a wide range of situations. In nature such flows are encountered in the oceans, lakes, solar pounds and the atmosphere. In industry, examples include chemical processes, crystal growth, energy storage, material processing as solidification, food processing, etc. For a review of the fundamental work in this area, see for instance Platten and Legros (1984) or Turner (1985).

Earlier studies on this topic are concerned with double-diffusive convection in a horizontal layer for which the flows, induced by the buoyancy forces, result from the imposition of both thermal and solutal boundary conditions on the horizontal walls. The onset of convection in binary mixtures were found to be very different from those reported in the past, in pure fluids. Thus, as discussed in details by Mamou et al. (2001), for instance, the onset of motion can arise at Rayleigh numbers below the supercritical value, indicating the development of subcritical flows. More recently, the onset of Soret-induced convection in a horizontal layer of a binary mixture, has been investigated by many authors. For this situation the mass fluxes within the layer result from the effect of thermal diffusion. A recent review of these studies is given by Ouriemi et al. (2005) for the case of layers of binary fluids under various boundary conditions. The case of porous layers saturated by binary solutions has been review by Bahloul et al. (2007).

Most available studies on this problem are concerned with the case of horizontal fluid layer bounded by rigid impervious walls. However, in many applications, the convective flow is in interaction with more complex boundary conditions such as by porous layers for instance. The interaction that occurs at the interface between a fluid and a porous medium has been formulated in the past according to two approaches. One approach is to use the Brinkman equation for the porous layer with the continuity of velocity and shear at the interface conditions. Using this model the linear stability theory was used by Somerton and Catton (1982) for the study of the onset of motion of fluid-saturated porous medium with internal heat generation overlaid with a fluid layer, and by Vasseur et al. (1989) for the analysis of the stability in a system consisting of a horizontal fluid layer over a layer of porous medium. The same problem was reconsidered recently by Hirta et al. (2007a,b), using both the so-called one-domain and two-domain approaches. The different treatment of the interfacial region is discussed by these authors. The influence of the stress jump boundary condition proposed by Ochoa-Tapia and Whitaker (1995a,b) has been investigated by Hirta et al. (2007a,b). The importance of the fluid-porous interfacial modeling was demonstrated. The other approach is to employ Darcy's equation for the porous layer with the slip conditions, proposed by Beavers and Joseph (1967) or Jones (1973), as one of the interfacial conditions. Nield (1967, 1983) applied the Beavers and Joseph boundary condition to study the thermal stability of superposed porous and fluid layers for various boundary conditions at the upper and lower of the system. Since then, the majority of linear stability analyses have been carried out using the slip boundary condition (Chen and Chen, 1988; Carr and Straughan, 2003; Carr, 2004; Shivakumara et al. 2006). The Beavers–Joseph model has also been

* Corresponding author. Tel.: +1 514 340 4711; fax: +1 514 340 5917.
E-mail address: zineddine.alloui@polymtl.ca (Z. Alloui).
URL: http://www.meca.polymtl.ca/convection (Z. Alloui).

0142-727X/$ - see front matter © 2008 Elsevier Inc. All rights reserved.
doi:10.1016/j.ijheatfluidflow.2008.03.016

Nomenclature

A	aspect ratio of the cavity, (L'/H')
D	mass diffusivity of species, m^2/K
D'	thermodiffusion coefficient, $m^2/s\ K$
Da	Darcy-number K/H'^2
Da^*	modified Darcy-number $\sqrt{Da}/\alpha^*$
g	gravitational acceleration, m/s^2
H'	height of fluid layer, m
j'	constant mass flux per unit area, kg/m s
k	thermal conductivity, W/(m K)
L'	width of fluid layer, m
Le	Lewis number, (α/D)
N	mass fraction
N_0	reference mass fraction
Nu	Nusselt number, Eq. (18)
Pr	Prandtl number, ν/α
q'	constant heat flux per unit area, W/m^2
Ra_S	solutal Rayleigh number, $Ra_T \varphi Le$
Ra_T	thermal Rayleigh number, $g\beta'_T \Delta T' H'^3/\alpha\nu$
Ra_{TC}^{sub}	subcritical Rayleigh number, Eq. (38)
Ra_{TC}^{sup}	supercritical Rayleigh number, Eq. (37)
S	normalized mass fraction, $N/\Delta N$
Sh	Sherwood number, Eq. (19)
t	dimensionless time, $t'\alpha/H'^2$
T	dimensionless temperature, $(T' - T'_0)/\Delta T'$
u	dimensionless velocity in x-direction, $(u'H'/\alpha)$
v	dimensionless velocity in y-direction, $(v'H'/\alpha)$
x	dimensionless coordinate axis, (x'/H')
y	dimensionless coordinate axis, (y'/H')

Greek symbols

α	thermal diffusivity, m^2/s
α^*	empirical dimensionless slip coefficient
β_N	concentration expansion coefficient
β'_T	thermal expansion coefficient, K^{-1}
ν	kinematic viscosity of fluid, m^2/s
ϕ	buoyancy ratio, $(\beta_N \Delta N/\beta'_T \Delta T')$
ρ	density of fluid, kg/m^3
Ψ	dimensionless stream function, Ψ'/α

Subscript

0	reference state

Superscript

$'$	refers to dimensional variable

used in the past to investigate natural convection within systems of superposed porous and fluid layers. Poulikakos et al. (1986) reported a numerical analysis of high Rayleigh convection for the case of a fluid layer on top of a porous layer. The effects of combined Marangoni and Rayleigh convections in a liquid layer, underlain by a porous layer, have been considered by Saghir et al. (2002). Results indicate that the Marangoni convection enhances the flow in the liquid layer but reduces the convection in the porous layer.

All the above studies are concerned with the effects of the interfacial conditions on the convective motion within a system of superposed porous and fluid layers. When the fluid is pure the resulting flows are induced by a single buoyancy force, namely temperature gradients. Binary mixtures are encountered in many practical situations such as in petroleum extraction, underground diffusion of nuclear waste, oil reservoir analysis and separation of mixtures. For instance water–ethanol mixtures are typical materials present in a wide range of areas, such as oil reservoirs (Saghir et al., 2004). The purpose of the present work is to investigate natural convection in a horizontal layer of a binary mixture bounded by two thin porous layers. The fluid layer is assumed to be heated and salted from the bottom by constant fluxes and to be shallow. Under these conditions, approximate analytical solutions for unicellular convection in the central part of the layer can be obtained using a parallel flow assumption. Results are presented for the onset of motion and the convective heat and mass transfers in terms of the governing parameters of the problem. Also, the stability of the parallel flow regime is investigated numerically in order to predict the critical Rayleigh number for Hopf's bifurcation.

2. Mathematical formulation

The configuration considered in this study is a horizontal shallow cavity, of thickness H' and width L' filled with a binary mixture and bounded by thin horizontal porous layers (see Fig. 1). The origin of the coordinate system is located at the center of the cavity with x' and y' being the horizontal and vertical coordinates, respectively. All the boundaries are impermeable. Neumann boundary conditions are applied, for both temperature and concentration, on the horizontal walls of the layer. The binary fluid is assumed

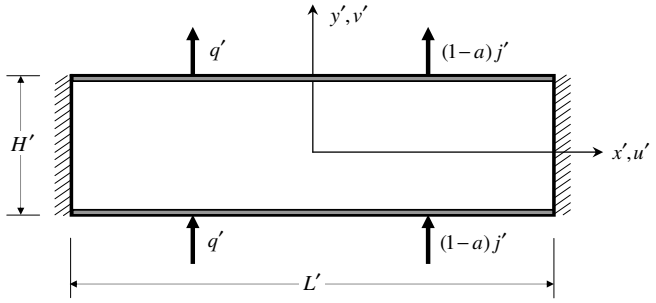

Fig. 1. Schematic diagram of the problem domain and coordinate system.

to satisfy the Boussinesq approximation. The density variation with temperature and concentration is described by the state equation $\rho = \rho_0[1 - \beta'_T(T' - T'_0) - \beta_N(N - N_0)]$ where ρ_0 is the fluid mixture density at temperature $T' = T'_0$ and mass fraction $N = N_0$ and β'_T and β_N are the thermal and concentration expansion coefficients, respectively.

The equations relating the fluxes of heat, $\vec{Q}'$, and matter, $\vec{J}'$, to the thermal and solute gradients present in the binary fluid mixture are given by (see for instance, De Groot and Mazur, 1962)

$$\vec{Q}' = -k\nabla T', \quad \vec{J}' = -\rho D\nabla N - \rho D' N_0(1 - N_0)\nabla T' \tag{1}$$

where k and D are the thermal conductivity and the isothermal diffusion coefficient. D' is the coefficient for the Soret effect.

The governing equations which describe the system behaviour are conservation of momentum, energy and species which are given below in terms of the stream function Ψ' as

$$\frac{\partial(\nabla^2\Psi')}{\partial t'} + J(\Psi', \nabla^2\Psi') = \nu\nabla^4\Psi' - \frac{g\beta'_T}{\nu}\frac{\partial}{\partial x'}\left(T' + \frac{\beta_N}{\beta'_T}N\right) \tag{2}$$

$$\frac{\partial T'}{\partial t'} + J(\Psi', T') = \alpha\nabla^2 T' \tag{3}$$

$$\frac{\partial N}{\partial t'} + J(\Psi', N) = D\nabla^2 N + aD' N_0(1 - N_0)\nabla^2 T' \tag{4}$$

where, as usual, in order to satisfy the continuity equation, the stream function Ψ' is defined such that $u' = \partial\Psi'/\partial y'$, $v' = -\partial\Psi'/\partial x'$ and $J(f,g) = \partial f/\partial y\ \partial g/\partial x - \partial f/\partial x\ \partial g/\partial y$.

The hydrodynamic boundary conditions applied on the walls of the layer are

$$x' = \pm L'/2 \quad \Psi' = 0 \quad \frac{\partial \Psi'}{\partial x'} = 0 \tag{5}$$

$$y' = -H'/2 \quad \Psi' = 0 \quad \frac{d^2\Psi'}{dy'^2} = \frac{\alpha_1^*}{\sqrt{K}}\frac{d\Psi'}{dy'} \tag{6}$$

$$y' = H'/2 \quad \Psi' = 0 \quad \frac{d^2\Psi'}{dy'^2} = \frac{-\alpha_2^*}{\sqrt{K}}\frac{d\Psi'}{dy'} \tag{7}$$

where K is the permeability of the porous boundary and α^* is the dimensionless material constant called the slip parameter (Beavers and Joseph, 1967).

Eq. (5) expresses the non-slip boundary condition on solid boundaries while Eqs. (6) and (7) are the Beavers–Joseph conditions at the interface of the horizontal boundaries of the fluid layer.

The thermal and solutal boundary conditions applied on the wall of the layer are

$$x' = \pm L'/2 \qquad \frac{\partial T'}{\partial x'} = 0 \quad \frac{\partial N}{\partial x'} = 0 \tag{8}$$

$$y' = \pm H'/2 \qquad \frac{\partial T'}{\partial y'} = -\frac{q'}{k} \quad \frac{\partial N}{\partial y'} = \frac{j'(1-a)}{\rho D} - a\frac{D'}{D}N_0(1-N_0)\frac{\partial T'}{\partial y'} \tag{9}$$

The governing equations are nondimensionalized by scaling length by H', stream function by the thermal diffusivity α and time by α/H'^2. Also, we introduce the reduced temperature $T = (T' - T'_0)/\Delta T'$ and the reduced concentration $S = N/\Delta N$, where $\Delta T' = q'H'/k$ and $\Delta N = -j'/\rho D$ for double-diffusive convection and $\Delta N = N_0(1 - N_0)\Delta T' D'/D$ for Soret-driven convection. In the above expressions, q' and j' are uniform fluxes of heat and mass per unit area respectively, applied on the horizontal walls of the system and a real number, the significance of which will be discussed below.

The dimensionless equations governing the present problem then read

$$\frac{\partial \nabla^2\Psi}{\partial t} + J(\Psi, \nabla^2\Psi) = Pr\nabla^4\Psi - PrRa_T\left(\frac{\partial T}{\partial x} + \varphi\frac{\partial S}{\partial x}\right) \tag{10}$$

$$\frac{\partial T}{\partial t} + J(\Psi, T) = \nabla^2 T \tag{11}$$

$$\frac{\partial S}{\partial t} + J(\Psi, S) = \frac{1}{Le}(\nabla^2 S - a\nabla^2 T) \tag{12}$$

The corresponding boundary conditions are

$$x = \pm A/2 \quad \Psi = 0 \quad \frac{\partial \Psi}{\partial x} = 0 \tag{13}$$

$$y = -1/2 \quad \Psi = 0 \quad \frac{d^2\Psi}{dy^2} = \frac{1}{Da_1^*}\frac{d\Psi}{dy} \tag{14}$$

$$y = 1/2 \quad \Psi = 0 \quad \frac{d^2\Psi}{dy^2} = \frac{-1}{Da_2^*}\frac{d\Psi}{dy} \tag{15}$$

$$x = \pm A/2 \quad \frac{\partial T}{\partial x} = 0 \quad \frac{\partial S}{\partial x} = 0 \tag{16}$$

$$y = \pm 1/2 \quad \frac{\partial T}{\partial y} = -1 \quad \frac{\partial S}{\partial y} = (a-1) + a\frac{\partial T}{\partial y} \tag{17}$$

From the above equations it is observed that the present problem is governed by the thermal Rayleigh number $Ra_T = g\beta'_T\Delta T' H'^3/\alpha\nu$, buoyancy ratio $\varphi = \beta_N\Delta N/\beta'_T\Delta T'$, Lewis number $Le = \alpha/D$, Prandtl number $Pr = \nu/\alpha$, aspect ratio $A = L'/H'$, modified Darcy-number $Da^* = \sqrt{Da}/\alpha^*$ and parameter a.

The case $a = 0$ corresponds to double-diffusive convection for which the solutal buoyancy forces in the liquid layer are induced by the imposition of a constant mass flux q' such that $\partial T/\partial y = -1$ on the vertical boundaries. According to Eq. (17) the corresponding solutal boundary conditions are given by $\partial S/\partial y = -1$. On the other hand $a = 1$ corresponds to the case of a binary fluid subjects to the Soret effect.

In the present study the intensity of the thermal buoyancy force and its relation to solutal buoyancy force are expressed in terms of parameter Ra_T and φ. The heat and mass transfer rates can be expressed in terms of the Nusselt and Sherwood numbers, and can be obtained from the following expressions:

$$Nu = \frac{q'}{k\Delta T'/H'} = \frac{1}{\Delta T} \tag{18}$$

$$Sh = \frac{j'}{D\Delta N/H'} = \frac{1}{\Delta S} \tag{19}$$

where $\Delta T = T(0,-1/2) - T(0,1/2)$ and $\Delta S = S(0,-1/2) - S(0,1/2)$ are the temperature and concentration differences, evaluated at $x = 0$. This follows from the fact that ΔT and ΔS are independent of x, such that they are arbitrarily evaluated at the center of the cavity.

3. Numerical solution

The solution of the governing equations and boundary conditions, Eqs. (10)–(12), is obtained using a control volume approach and SIMPLER algorithm (Patankar,1980). A finite difference procedure with variable grid size is considered for better consideration of boundary conditions. The power-law scheme is used to evaluate the flow, heat and mass fluxes across each of the control volume boundaries. A second order back-wards finite difference scheme is employed to discretize the temporal terms appearing in the governing equations (see Ouriemi et al. (2005) for more details).

A line-by-line tridiagonal matrix algorithm with relaxation is used in conjunction with iterations to solve the non-linear discretized equations. We consider that convergence is reached when

$$\frac{\sum_i\sum_j|\Psi_{i,j}^{n+1} - \Psi_{i,j}^{n}|}{\sum_i\sum_j|\Psi_{i,j}^{n+1}|} \leqslant 10^{-6} \tag{20}$$

where the superscripts n and $(n+1)$ indicate the value of the nth and $(n+1)$th iterations, respectively, i and j indices denote grid location in the (x,y) plane. Numerical tests, using various mesh sizes, were done for the same conditions in order to determine the best compromise between accuracy of the results and computer time. Thus, most of the calculations presented in this paper were performed using a 60×180 grid.

As discussed above the present problem depends upon the parameters Ra_T, φ, Le, Pr, α^*, Da, A and a. The numerical results presented in this study were obtained for $Pr = 7$ and $A = 8$. Such an aspect ratio is large enough to approximate the parallel flow model describe in the following section. It is well known that the slip coefficient α^*, in Eqs. (6) and (7), depends on the porosity and the structure of the porosity of the porous medium, varying from 0.1 to 4 (Beavers and Joseph, 1967). Therefore, in the present study, the effect of α^* was examined over a range $0 \leqslant \alpha^* \leqslant 10$. Furthermore, in order not to violate the Darcy flow model, the Darcy-number values have been restricted to the 10^{-8}–10^{-4} range. With these values, the range of the modified Darcy-number $Da^* = \sqrt{Da}/\alpha^*$ extends from almost zero to infinity.

Typical numerical results are presented in Fig. 2a and b for $Ra_T = 1000$, $Le = 10$, $\varphi = 0.2$, $A = 6$ and $a = 0$ (double-diffusive-driven convection). On the graph, streamlines, isotherms and isoconcentrates are presented from top to bottom Fig. 2a) corresponds to the case $Da_1^* = Da_2^* = 0$, for which the upper and lower boundaries correspond to solid walls. This situation has been investigated in

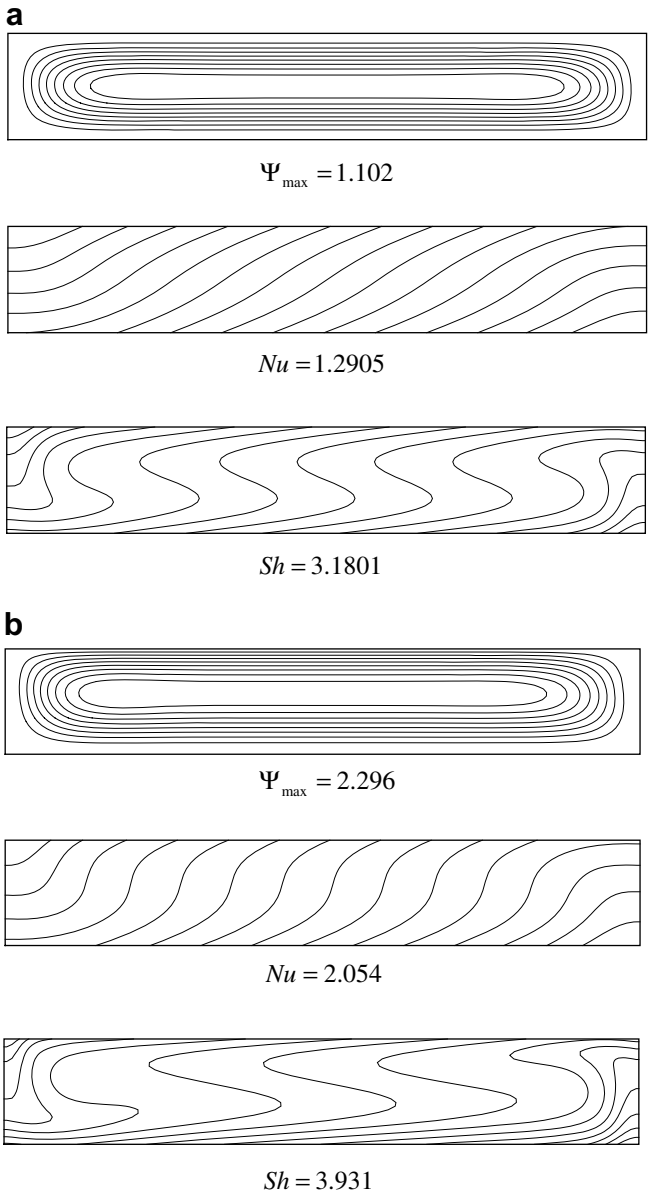

Fig. 2. Contour lines of stream function (top), temperature (center) and concentration (bottom) for $Ra_T = 10^3$, $Le = 10$, $\varphi = 0.2$, $a = 0$, $Da_1^* = 0$ and: (a) $Da_2^* = 0$ $\Psi_{max} = 1.102$, $Nu = 1.2905$, $Sh = 3.1801$ and (b) $Da_2^* = \infty$, $\Psi_{max} = 2.296$, $Nu = 2.054$ and $Sh = 3.931$.

details in the past by Mamou et al. (2001). Fig. 2b is obtained for the case of solid lower boundary ($Da_1^* = 0$) and upper free surface ($Da_2^* = \infty$). As expected the intensity of the resulting flow pattern is enhanced and the symmetry of solution with respect to the center of the cavity is destroyed. These numerical results clearly indicate that for a shallow layer ($A \gg 1$) the flow in the core region of the enclosure is clearly parallel, while the temperature and concentration are linearly stratified in the horizontal direction. The analytical solution, developed in the following section, will rely on these observations.

4. Analytical solution

In the limit of a shallow cavity $A \gg 1$, the governing Eqs. (10)–(12) can be considerably simplified under the parallel flow assumption $\Psi(x,y) \approx \Psi(y), T(x,y) \approx C_T x + \theta_T(y) and S(x,y) \approx C_S x + \theta_S(y)$, where C_T and C_S are unknown constant temperature and concentration gradients respectively in x-direction (see for instance Ouriemi et al., 2005).

Using the above approximations, Eqs. (10)–(12) reduce to the following systems of equations:

$$\frac{d^4\Psi}{dy^4} = Ra_T(C_T + \varphi C_S) \tag{21}$$

$$\frac{d\Psi}{dy}C_T = \frac{d^2\theta_T}{dy^2} \tag{22}$$

$$\frac{d\Psi}{dy}C_S = \frac{1}{Le}\left[\frac{d^2\theta_S}{dy^2} - a\frac{d^2\theta_T}{dy^2}\right] \tag{23}$$

The solution of Eqs. (21)–(23), satisfying the boundary conditions 14, 15, and 17, is

$$\Psi = \Psi_0(4y^2 - 1)(4y^2 - 2L_1 - 8L_2 y + 1) \tag{24}$$

$$\theta_T = \frac{\Psi_0 C_T}{15} y(48y^4 - 10L_1(4y^2 - 3) - 60L_2(2y^3 - y) - 15) - y \tag{25}$$

$$\theta_S = \frac{\Psi_0(C_S Le + aC_T)}{15} y(48y^4 - 10L_1(4y^2 - 3) - 60L_2(2y^3 - y) - 15) - y \tag{26}$$

where $\Psi_0 = 15Ra_T^0(C_T + \varphi C_S)/8, Ra_T^0 = Ra_T/Ra_0^{sup}, Ra_0^{sup} = 720$ and the contribution of two modified Darcy-numbers are represented in terms of L_1 and L_2 defined as follows:

$$L_1 = (36Da_1^* Da_2^* + 6(Da_1^* + Da_2^*) + 1)/(12Da_1^* Da_2^* + 4(Da_1^* + Da_2^*) + 1) \tag{27}$$

$$L_2 = -(Da_1^* - Da_2^*)/(12Da_1^* Da_2^* + 4(Da_1^* + Da_2^*) + 1) \tag{28}$$

The effect of the return flow from the end regions is taken into account via a global balance (see Mamou et al., 2001, for instance). Making use of the boundary conditions, Eqs. (13) and (16), the temperature and concentration gradients C_T and C_S can be obtained as

$$C_T = \frac{B_2\Psi_0}{1 + B_1\Psi_0^2} \tag{29}$$

$$C_S = \frac{aC_T(Le + 1) + (1 - a)B_2 Le\Psi_0}{1 + B_1 Le^2\Psi_0^2} \tag{30}$$

where

$$B_1 = \frac{4}{45}\left(24L_1^2 - \frac{192}{7}L_1 + \frac{96}{7}L_2^2 + 8\right) \tag{31}$$

and $B_2 = 4(L_1/3 - 1/5)$ (32)

Substituting the above equations of C_T and C_S into the expression for Ψ_0, the following fifth order polynomial is obtained:

$$\Psi_0\left[(B_1^4 Le^4)\Psi_0^4 - (B_1^2 Le^2)d_1\Psi_0^2 - d_2/4\right] = 0 \tag{33}$$

where

$$d_1 = B_1\left[\frac{15}{8}Ra_T^0 B_2(Le^2 + \varphi Le(1 - a)) - Le^2 - 1\right] \tag{34}$$

$$d_2 = 4B_1^2 Le^2\left[\frac{15}{8}Ra_T^0 B_2(1 + \varphi(a + Le)) - 1\right] \tag{35}$$

The solution for Eq. (33) is explicitly expressed as follows:

$$\Psi_0 = \left\{\pm\frac{\sqrt{2}}{2B_1 Le}\left(d_1 \pm \sqrt{d_1^2 + d_2}\right)^{1/2}, 0\right\} \tag{36}$$

in which the solution $\Psi_0 = 0$ represents the pure conduction rest state and the four other solutions stand for convective solutions. Eq. (36) also leads us to the critical values for existence of convec-

tion in the layer. The supercritical Rayleigh number Ra_{TC}^{sup}, for the onset of motion from the rest state, is obtained, when the conditions $d_1 < 0$ and $d_2 = 0$ are satisfied, as

$$Ra_{TC}^{sup} = \frac{R_0}{(1+\varphi(a+Le))} \tag{37}$$

where $R_0 = 8Ra_0^{sup}/15B_2$.

In the present analysis, it can be demonstrated that subcritical flows with a finite-amplitude convection occur when $d_1 > 0$ and $d_1^2 + d_2 = 0$ (see Mamou et al., 2001) as

$$Ra_{TC}^{sub} = \frac{R_0(1+Le)}{Le[1+\varphi(1-a)]^2} \times \left[(Le-1)(Le-\varphi) - a\varphi(Le+1) + 2\sqrt{\varphi Le(Le+a-1)(a\varphi - Le+1)}\right] \tag{38}$$

The local heat and mass transfer rates are obtained according, to Eqs. (18), (19), (25), and (26), by

$$Nu = \frac{1}{1-B_2\Psi_0 C_T} \tag{39}$$

$$Sh = \frac{1}{1-B_2\Psi_0(C_S Le + aC_T)} \tag{40}$$

The above analytical solution can be checked against particular results for the following special cases.

4.1. Fluid layer bounded by two solid horizontal walls

For this situation $Da_1^* \to 0$ and $Da_2^* \to 0$ such that $L_1 = 1$, $L_2 = 0$, $B_1 = 128/315$, $B_2 = 8/15$ and $R_0 = 720$. Upon substituting these constants into Eqs. (24), (25), (26), (37), (38), (39), and (40) yields the solution obtained in the past by Ouriemi et al. (2005).

4.2. Fluid layer bounded by a solid wall and a free boundary

This situation is reached either for $Da_1^* \to 0$ and $Da_2^* \to \infty$ (or for $Da_1^* \to \infty$ and $Da_2^* \to 0$). The resulting constants are then given by $L_1 = 3/2$, $L_2 = 1/4$, $B_1 = 608/315$, $B_2 = 6/5$ and $R_0 = 320$. This situation is a particular case of the problem considered by Mahidjiba et al. (2006), i.e. flows in a fluid layer induced by the combined action of shear stress and the Soret effect.

4.3. Fluid layer bounded by two free surfaces

This situation occurs for $Da_1^* \to \infty$ and $Da_2^* \to \infty$. As a result it is found that $L_1 = 3$, $L_2 = 0$, $B_1 = 3968/315$, $B_2 = 16/5$ and $R_0 = 120$. For this situation, which has not been investigated in the literature, it is readily found that

$$\begin{aligned} \Psi &= \Psi_0(4y^2-1)(4y^2-5) \\ \theta_T &= \frac{\Psi_0 C_T}{15} y(48y^4 - 120y^2 + 75) - y \\ \theta_S &= \frac{\Psi_0(C_S Le + aC_T)}{15} y(48y^4 - 120y^2 + 75) - y \end{aligned} \tag{41}$$

where Ψ_0 is given by Eq. (36).

The supercritical and subcritical Rayleigh numbers are given by Eqs. (37) and (38) while the Nusselt and Sherwood numbers can be evaluated from Eqs. (39) and (40).

The distribution of the velocity component, u, temperature, T, and concentration, S, profiles in the vertical mid-plane ($x = 0$) of the cavity is illustrated in Fig. 3. This graph has been plotted for $Ra_T = 10^3$, $Le = 10$, $\varphi = 0.2$, $a = 0$, $Da_1^* = 0$ (solid lower boundary) and various values of Da_2^*. The result shows that the approximate model (solid lines), based on the parallel flow approximation, is in excellent agreement with the numerical solution of the full governing equations. The effect of the conditions imposed on the upper boundary is clearly observed from Fig. 3. The intensity of

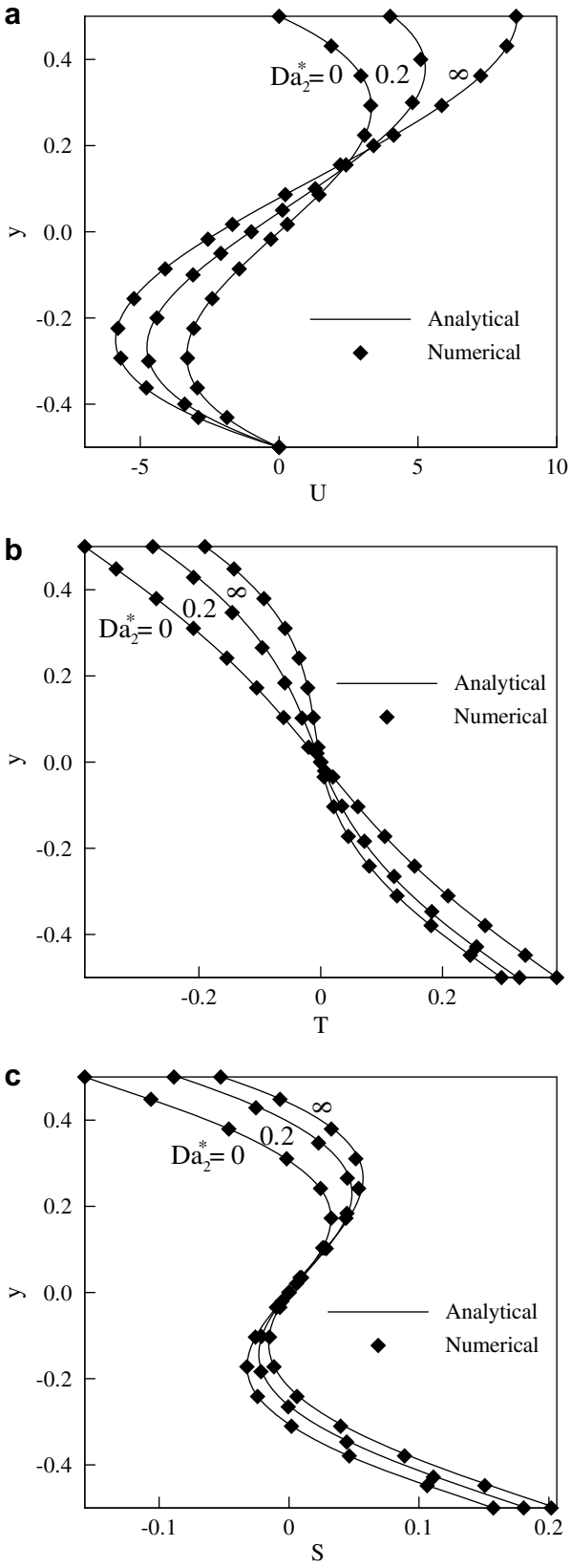

Fig. 3. Distribution of (a) horizontal velocity component, u, (b) temperature, T, and (c) concentration, S, profiles at the vertical mid-plan ($x = 0$) of the cavity for, $Ra_T = 10^3$, $Le = 10$, $\varphi = 0.2$, $a = 0$, $Da_1^* = 0$ and $Da_2 = 0, 0.2, \infty$.

the flow (velocity) increases considerably near the upper surface when Da_2^* increases from zero (solid boundary) to infinity (free upper surface). The influence of Da_2^* on T and S is also found to be significant.

Fig. 4 exemplifies the effect of parameter Da_2^* on the bifurcation diagram in terms of Ψ_{max} the maximum value of the streamfunction as a function of Ra_T for $\varphi = 0.2$, $Le = 2$, $Da_1^* = 0$ and $a = 0$ and 1. The curves depicted in the graphs are the prediction of the parallel flow approximation. The numerical solution of the full governing equations, obtained for $A = 8$ and $Pr = 7$ are depicted by dots and are seen to be, here again, in good agreement with the analytical solution. The results presented in Fig. 4 are obtained for $\varphi > 0$, namely $\varphi = 0.2$, for which the thermal and solutal buoyancy forces are destabilizing. For this situation it is well know that, as discussed by many author (see Mamou et al. (2001), for instance), the onset of convection occurs through a pitchfork bifurcation. Thus, for $Da_2^* = 0$, i.e. for a fluid layer bounded by solid walls, transition from the rest state occurs at a supercritical Rayleigh number $Ra_{TC}^{sup} = 514.3$ for double-diffusive convection ($a = 0$) and $Ra_{TC}^{sup} = 450$ for Soret-induced convection. The case $Da_2^* \gg 1$ corresponds to a fluid layer with a free boundary condition for which $Ra_{TC}^{sup} = 228.6$ for $a = 0$ and $Ra_{TC}^{sup} = 200$ for $a = 1$. Curves for intermediate values of Da_2^*, namely $Da_2^* = 0.05$ and 0.5 are also presented in Fig. 4 to illustrate the influence of this boundary condition on the present problem.

The results obtained for $\varphi < 0$, namely $\varphi = -0.2$, are presented in Fig. 5, for the same other conditions as those of Fig. 4. For this situation the thermal and solutal forces are opposing each other and the graphs indicate the occurrence of subcritical bifurcation curves, as predicted by Eq. (38). For the conditions considered here when $Da_2^* = 0$ the onset of convection are $Ra_{TC}^{sub} = 1155.6$ for $a = 0$ and $Ra_{TC}^{sub} = 1285.2$ for $a = 1$. Similarly, when $Da_2^* = \infty$, $Ra_{TC}^{sub} = 514.08$ for $a = 0$ and $Ra_{TC}^{sub} = 571.68$ for $a = 1$. The result obtained for $Ra_T < 0$ (not presented here), corresponding to the case of a cavity heated from the top indicate that convection occurs through a pitchfork situation at a supercritical Rayleigh number given by Eq. (37).

5. Linear stability analysis

A linear stability analysis is presented in this section to determine the criterion for the onset of oscillatory convection.

We consider the convective flows predicted by the parallel flow approximation Eqs. (24)–(26). This flow is not expected to remain

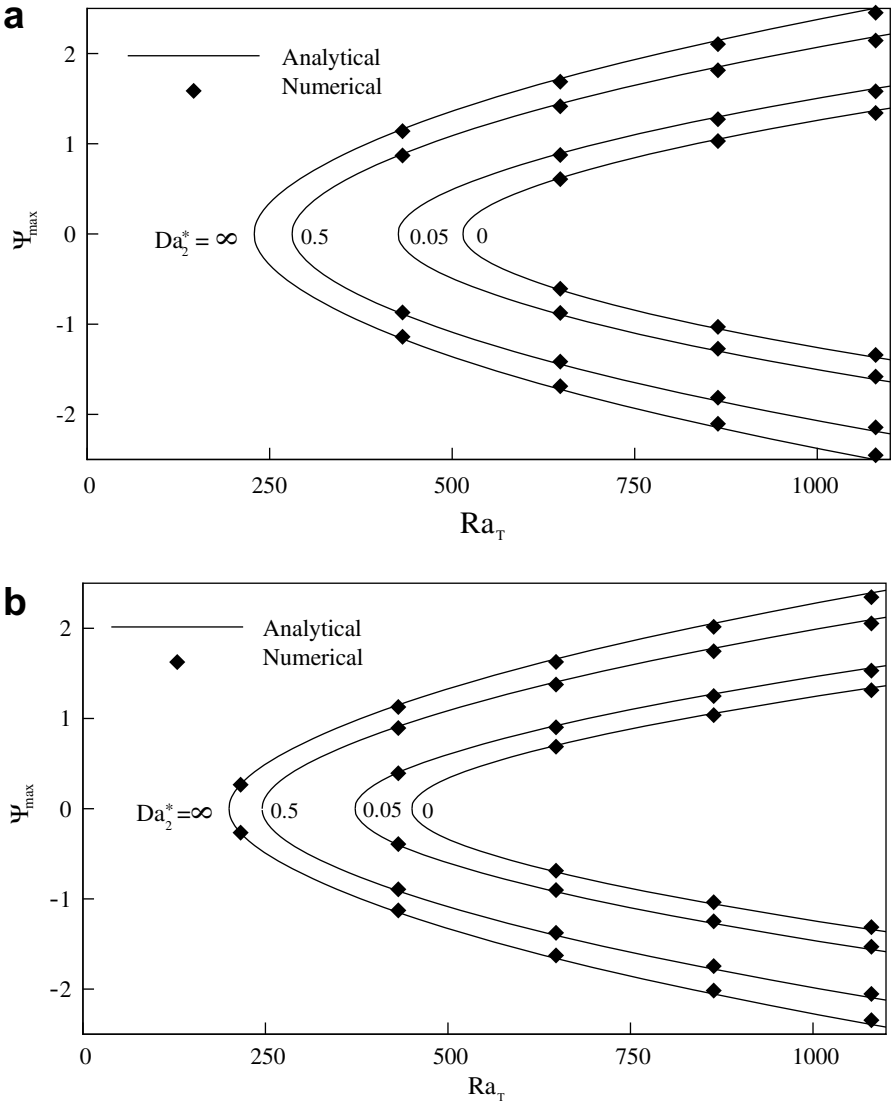

Fig. 4. Bifurcation diagrams in terms of Ψ_{max} versus Ra_T for various values of Da_2^* and $Le = 2$, $\varphi = 0.2$ and (a) $a = 0$ and (b) $a = 1$.

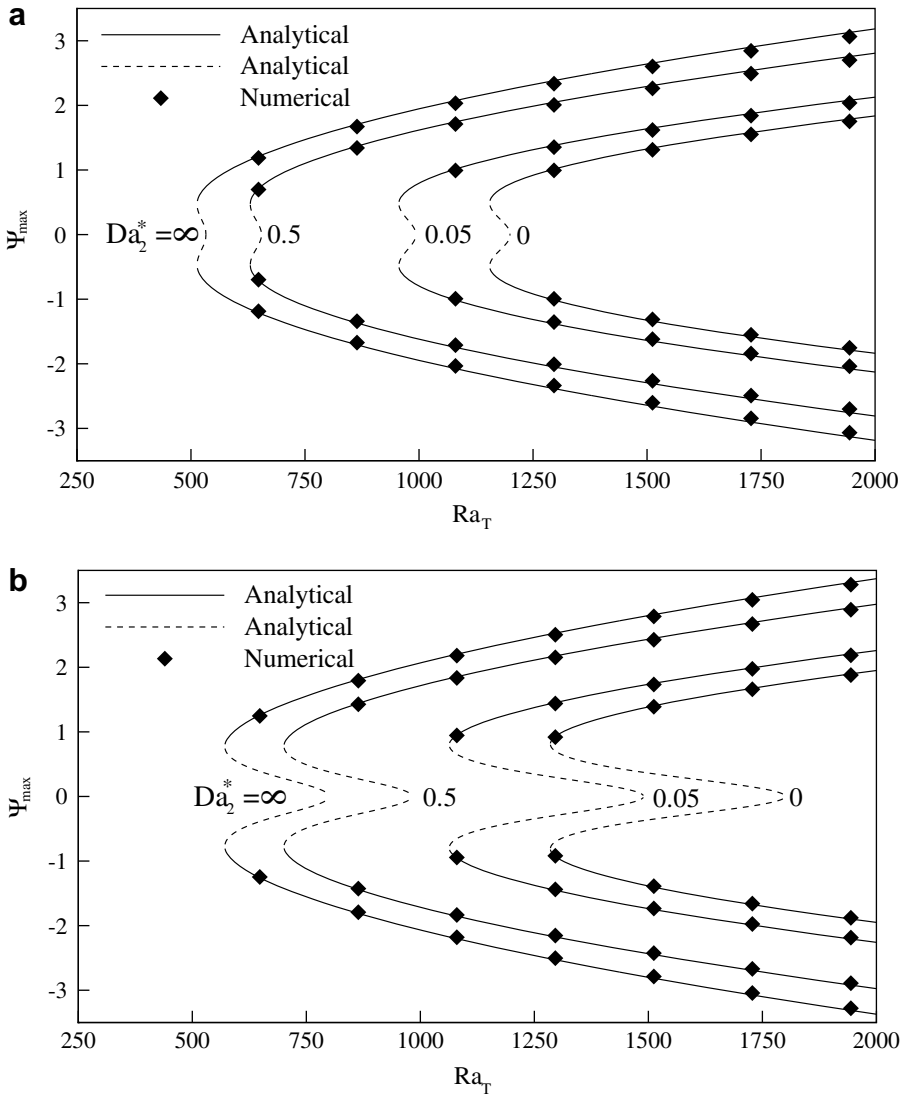

Fig. 5. Bifurcation diagrams in terms of Ψ_{max} versus Ra_T for various values of Da_2^* and $Le = 2$, $\varphi = -0.2$ and (a) $a = 0$ and (b) $a = 1$.

steady independently of the range of the governing parameters. In fact, when the intensity of the flow is increased above a critical value it becomes instable. At the very beginning of instability, the global flow can be assumed to be a superposition of the basic flow $[\Psi(x,y) \approx \Psi(y), T(x,y) \approx C_T x + \theta_T(y) and S(x,y) \approx C_S x + \theta_S(y)]$ and an infinitesimal perturbation. Thus, we have

$$\left.\begin{aligned}\hat{\psi}(t,x,y) &= \tilde{\psi}(y)e^{pt+ikx}\\ \hat{\theta}_T(t,x,y) &= \tilde{\theta}_T(y)e^{pt+ikx}\\ \hat{\theta}_S(t,x,y) &= \tilde{\theta}_S(y)e^{pt+ikx}\end{aligned}\right\} \tag{42}$$

where $p = \sigma + i\omega$ is the complex amplification rate of the perturbation, k is the real wave number and ω the frequency.

Substitution of the sum of the base flow and perturbation variables, into the set of governing Eqs. (10)–(12), followed by linearization to first-order in small quantities, yields the following system of equations:

$$\begin{aligned}&Pr(D^4 + k^4)\tilde{\psi} - ikD^3\psi\tilde{\psi} + ik(D^2 - k^2)D\psi\tilde{\psi}\\ &\quad - ikPr\left(Ra_T\tilde{\theta}_T + \frac{Ra_S}{Le}\tilde{\theta}_S\right)D\tilde{\psi}\\ &\quad = p(D^2 - k^2)\tilde{\psi}\end{aligned} \tag{43}$$

$$(D^2 - k^2)\tilde{\theta}_T - ikD\psi\tilde{\theta}_T - C_T D\tilde{\psi} + ikD\theta_T\tilde{\psi} = p\theta_T \tag{44}$$

$$\frac{1}{Le}(D^2 - k^2)(\tilde{\theta}_S - a\tilde{\theta}_T) - ikD\psi\tilde{\theta}_S - C_S D\tilde{\psi} + ikD\theta_S\tilde{\psi} = p\theta_S \tag{45}$$

where $Ra_S = Ra_T\varphi Le$ is the solutal Rayleigh number.

The corresponding boundary conditions are

$$y = -1/2, \quad \tilde{\psi} = 0; \quad D^2\tilde{\psi} = (1/Da_1^*)D\tilde{\psi}; \quad D\tilde{\theta}_T = D\tilde{\theta}_S = 0 \tag{46}$$

$$y = 1/2, \quad \tilde{\psi} = 0; \quad D^2\tilde{\psi} = (-1/Da_2^*)D\tilde{\psi}; \quad D\tilde{\theta}_T = D\tilde{\theta}_S = 0 \tag{47}$$

where $D = d/dy$.The perturbed state Eqs. (43)–(45) with the boundary conditions (46) and (47) may be written in a compact matrix form as

$$L(k)\mathbf{Y} = pM(k)\mathbf{Y} \tag{48}$$

where $\mathbf{Y} = [\tilde{\psi}, \tilde{\theta}_T, \tilde{\theta}_S]$ is a three-component vector of the perturbation and $L(k)$ and $M(k)$ are two linear differential operators that depend on the control parameters $Ra_T, Ra_S, Le, Pr, a, Da_1^*$ and Da_2^*.

The set of Eq. (48) is solved using a finite differences scheme. Five-point central schemes for spatial discretization in the domain between $y = -1/2$ and $y = 1/2$. For N computational points, the resulting discrete system has $3N$ eigenvalues that can be found

using a standard IMSL subroutine such as DGVCCG. The details of the numerical procedure are discussed in details by Bahloul et al. (2003) and thus not presented here.

The validation of the present stability analysis can be made for the case considered by Prud'homme and Hung Nguyen (2002) for the particular case of pure fluid layer ($Ra_S = 0$), bounded by solid boundaries ($Da_1^* = Da_2^* = 0$). The critical values obtained by these authors, displayed in Table 1, are observed to be in excellent agreement with the results of the numerical procedure described above.

As predicted by the parallel flow theory the onset of motion of the rest state of the present system occurs at a supercritical Rayleigh number given by $Ra_{TC}^{sup}[1 + \varphi(a + Le)] = R_0$. Fig. 6 illustrates the influence of parameters Da_1^* and Da_2^*, i.e. the slip conditions at the interface of the fluid layer, on the onset of motion. The parallel flow theory, displayed by solid lines, are seen to be in excellent agreement with the numerical solution of the linear stability theory predicted in this section for the particular case $\Psi = 0$ i.e. the rest state. As expected, it is observed from Fig. 6 that $R_0 = 720$ as Da_1^* and Da_2^* are made small enough. This result is in agreement with the predictions of Sparrow et al. (1964) for the case of a fluid layer bounded by rigid walls. Also, the value $R_0 = 120$, corresponding to the case of a fluid layer with free boundary conditions is recovered in the limit $Da_1^* \to \infty$ and $Da_2^* \to \infty$. Furthermore, the case of a fluid layer bounded by a solid horizontal boundary on one side and a free surface on the other side is recovered in the limit $Da_1^* \to \infty$ and $Da_2^* \to 0$ or $Da_1^* \to 0$ and $Da_2^* \to \infty$. For this situation $R_0 = 320$ as reported in the past by Sparrow et al. (1964). For intermediate value of Da_1^* and Da_2^* Fig. 6 shows a smooth transition of R_0 between the limits discussed above.

With the linear stability analysis discussed above it is possible to predict numerically the conditions for which the steady convection, predicted by the parallel flow theory, eventually becomes unstable. The transition, called Hopf's bifurcation, occurs at a critical Rayleigh number Ra_{TC}^{Hopf} which depends upon the value of the governing parameters, namely Ra_S, Le, Pr, a, Da_1^* and Da_2^*. Fig. 7 illustrates the influence of the Prandtl number Pr and solutal Rayleigh number Ra_S on the critical Rayleigh number Ra_{TC}^{Hopf} for the case of a fluid layer bounded by solid boundaries ($Da_1^* \to 0$ and $Da_2^* \to 0$). The curve corresponding to $Ra_S = 0$ will be discussed first. For this situation, considered in the past by Prud'homme and Hung Nguyen (2002), convection in the fluid layer is induced solely by the temperature gradients. As discussed by these authors the resulting curve indicates that Ra_{TC}^{Hopf} increases considerably as the value of Pr is made smaller. This results from that the fact the dissipation of the thermal perturbations, at the origin of the flow instability regime, is enhanced as Pr is made small (i.e. the thermal diffusivity is increased). Consequently a higher critical Rayleigh number (i.e. stronger heat flux at the bottom boundary) is required to destabilize the flow. For large Prandtl numbers ($Pr \geqslant 500$) the results indicate that Ra_{TC}^{Hopf} reaches an asymptotic value. For intermediate values of Pr it is observed that Ra_{TC}^{Hopf} reaches a minimum value for $Pr = 0$ (1). The way that the critical Hopf Rayleigh number is affected by the presence of solutal buoyancy forces is depicted in Fig. 7 for both the cases of double-diffusive convection ($a = 0$) and Soret-induced convection ($a = 1$). The curves for $Ra_S = 10^4$ correspond to a situation for which both the thermal and the solutal buoyancy forces are destabilizing. As a result the onset of the flow instability occurs at lower values than those obtained for the pure thermal situation ($Ra_S = 0$). Naturally, the reverse situation is observed for $Ra_S = -10^4$, i.e. when the thermal and solutal buoyancy forces are opposing each other. The critical Rayleigh number for the onset of Hopf bifurcation can also be estimated by the numerical solution of the full governing equations. Thus, for double-diffusive convection ($a = 0$) it was found that, for $\varphi = 0.2$, $Le = 2$, $Pr = 1$ and $A = 10$, the transition from steady to oscillatory convection occurs approximately at $Ra_{TC}^{Hopf} \simeq 39000$. This result is in good agreement with the value $Ra_{TC}^{Hopf} \simeq 37446$, predicted by the present linear stability analysis.

The influence of the slip coefficient parameters in the Beavers–Joseph condition, α_1^* and α_2^* on the stability of the convective flow predicted by the parallel flow approximation, Ra_{TC}^{Hopf}, is illustrated in Fig. 8 for $Da_1 = Da_2 = 10^{-6}$ and $Ra_S = 0$. As expected Ra_{TC}^{Hopf} is minimum when both α_1^* and α_2^* tend towards zero, i.e. for the case

Table 1
Validation of the numerical code, for $Ra_S = 0$ and $Da_1^* = Da_2^* = 0$, in terms of Ra_{TC}^{Hopf}, k_C and ω_C

	Prud'homme and Hung Nguyen (2002)			Present work		
Pr	Ra_{TC}^{Hopf}	k_C	ω_C	Ra_{TC}^{Hopf}	k_C	ω_C
50	64276	4.626	183.9	64276	4.626	183.9
100	65126	4.662	187.1	65126	4.662	187.1
500	65819	4.691	189.8	65819	4.691	189.8
5000	65977	4.697	190.4	65977	4.697	190.4

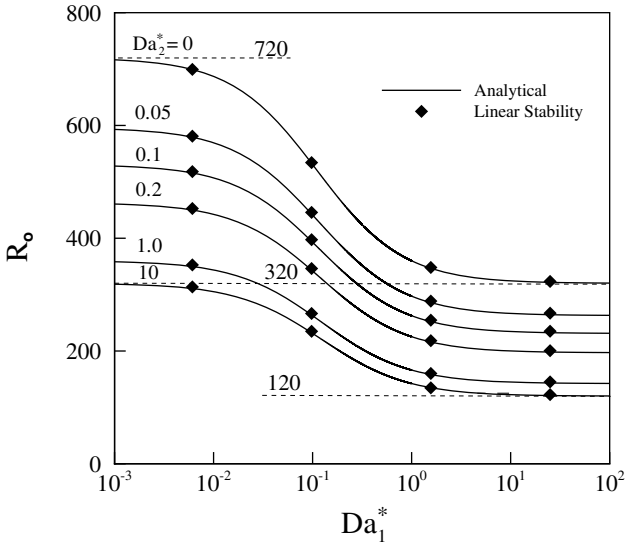

Fig. 6. Parameter R_0 as a function of Da_1^* and Da_2^*.

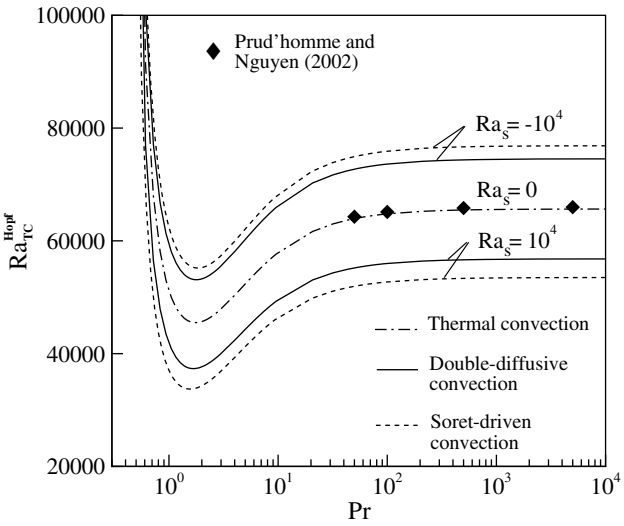

Fig. 7. Onset of oscillatory convection, Ra_{TC}^{Hopf}, as a function of Pr and Ra_S for $Le = 2$ and $Da_1^* = Da_2^* = 0$.

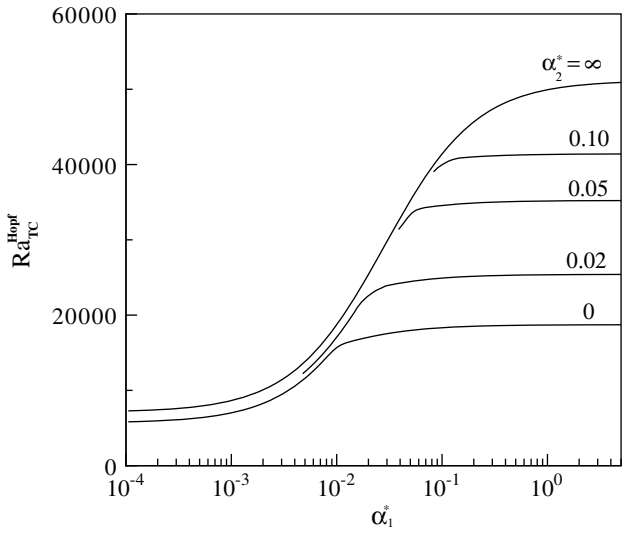

Fig. 8. Influence of the slip coefficient parameter in Beavers–Joseph condition, α_1^* and α_2^*, on the onset of oscillatory convection, Ra_{TC}^{Hopf}, for $Da_1 = Da_2 = 10^{-6}$, $a = 0$ and $Ra_S = 0$.

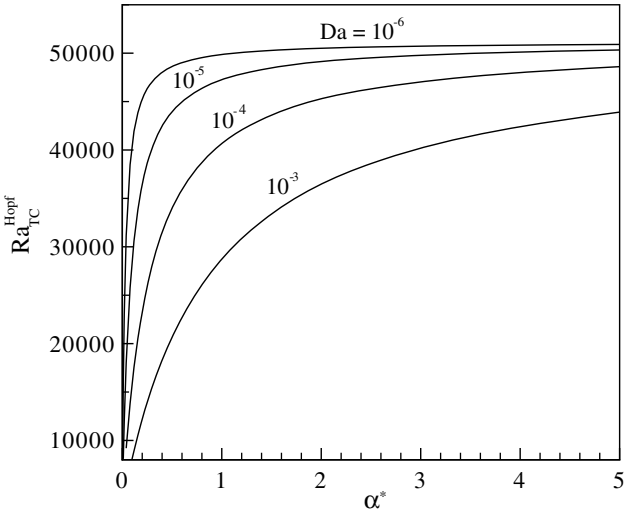

Fig. 9. Influence of the Darcy-number, $Da_1 = Da_2 = Da$, on the of oscillatory convection, Ra_{TC}^{Hopf}, as a function of $\alpha_1^* = \alpha_2^* = \alpha^*$ for $a = 0$and $Ra_S = 0$.

of fluid layer with free upper and lower boundary conditions. Naturally, Ra_{TC}^{Hopf} is maximum when the fluid layer is bounded by solid horizontal walls, for which α_1^* and α_2^* tend towards large values. Furthermore it is seen that the influence of α_2^* is considerable when α_1^* is relative large, for which an increase of α_2^* indicates a transition between rigid–free and rigid–rigid boundary conditions. However, the influence of α_2^* on the transition between free–free and free–rigid boundaries ($\alpha_1^* \to 0$) is found to be considerably less important.

Fig. 9 illustrates the influence of parameter $\alpha^* = \alpha_1^* = \alpha_2^*$ on Ra_{TC}^{Hopf} for various values of Da and when $Ra_S = 0$. The curves indicate that a decrease in Da results in an increases of the critical Rayleigh number for the onset of oscillatory convection, Ra_{TC}^{Hopf}. This is because a decrease of the Darcy-number implies a low permeable porous lining. This causes a damping of the fluid motion, requiring a large critical Rayleigh number to destabilize the steady convective flow. Also, it is observed that the influence of Da is considerably reduced as the value of α^* is made larger.

6. Conclusions

The present paper is devoted to the onset and development of convection in a horizontal layer of a binary fluid bounded by thin porous layers. The Beavers–Joseph (BJ) condition is employed to model the boundary condition at fluid/porous interface. Both the case of double-diffusion convection ($a = 0$) and Soret-driven convection ($a = 1$) are considered. The analytical solution, based on a parallel flow approximation, reveals in closed form, the role played by the BJ-slip condition at the interface Da_1^* and Da_2^*, thermal Rayleigh number Ra_T, buoyancy ratio φ, Lewis number Le and the type of convection (i.e. parameter a) considered. The main conclusions of the present analysis are:

(i) The analytical model derived in this study yields, for aiding flow ($\varphi > 0$), the supercritical Rayleigh number for the onset of convection from the rest state in terms of the BJ-slip condition. The prediction of the critical Rayleigh number is correctly obtained from the present parallel flow approximation because convection occurs at zero wave number when Neumann boundary conditions are applied on the boundaries. For opposing buoyancy forces ($\varphi < 0$) the model predicts the existence of a subcritical Rayleigh number, when the flow bifurcates from the rest state through finite-amplitude convection. An explicit expression for the subcritical Rayleigh number is obtained in terms of φ, Le, Da_1^*, Da_2^* and a. For finite-amplitude convection, useful expressions have been obtained for velocity, temperature and solute distributions in the core of the layer. The main features predicted by the analytical solution are confirmed by numerical solutions of the full governing equations.

(ii) The stability of the convective motion, predicted by the parallel flow approximation, has been investigated numerically on the bases of the linear stability theory. It has been found that the critical Rayleigh number for the onset of Hopf bifurcation depends upon φ, Le, Pr, Da_1^* and Da_2^*.

References

Bahloul, A., Boutana, N., Vasseur, P., 2003. Double-diffusive and Soret-induced convection in a shallow horizontal porous layer. Journal of Fluid Mechanics 491, 325–352.

Bahloul, A., Vasseur, P., Robillard, L., 2007. Convection of a binary fluid saturating a shallow porous cavity subjected to cross heat fluxes. Journal of Fluid Mechanics 574, 317–342.

Beavers, G.S., Joseph, D.D., 1967. Boundary conditions at a naturally permeable wall. Journal of Fluid Mechanics 30, 197–207.

Carr, M., 2004. Penetrative convection in a superposed porous-medium-fluid layer via internal heating. Journal of Fluid Mechanics 509, 305.

Carr, M., Straughan, B., 2003. Penetrative convection in a fluid overlying a porous layer. Advances in Water Resources 26, 26.

Chen, F., Chen, C.F., 1988. Onset of finger convection in a horizontal porous layer underlying a fluid layer. Journal of Heat Transfer 110, 403.

De Groot, S.R., Mazur, P., 1962. Nonequilibrium Thermodynamics. North-Holland, Amsterdam.

Hirata, S.C., Goyeau, B., Gobin, D., Carr, M., Cotta, R.M., 2007a. Stability analysis of natural convection in adjacent fluid and porous layers: influence of the interfacial modeling. International Journal of Heat and Mass Transfer 50, 1356.

Hirata, S.C., Goyeau, B., Gobin, D., 2007b. Stability of natural convection in superposed fluid and porous layers: influence of the interfacial jump boundary condition. Physics of Fluids 19. doi:10.1063/1.273087.

Jones, I.P., 1973. Low Reynolds number flow past a porous spherical shell. Proceedings of the Cambridge Philosophical Society 73, 231–238.

Mahidjiba, A., Bennacer, R., Vasseur, P., 2006. Flows in a fluid layer induced by the combined action of a shear stress and the Soret effect. International Journal of Heat and Mass Transfer 49, 1403–1411.

Mamou, M., Vasseur, P., Hasnaoui, M., 2001. On numerical stability analysis of double-diffusive convection in confined enclosures. Journal of Fluid Mechanics 433, 209–250.

Nield, D.A., 1967. Onset of convection in a fluid layer overlying a layer of porous medium. Journal of Fluid Mechanics 81, 513–522.

Nield, D.A., 1983. Boundary correction for the Rayleigh–Darcy problem: limitations of the Brinkman equation. Journal of Fluid Mechanics 128, 37–46.

Ochoa-Tapia, J.A., Whitaker, S., 1995a. Momentum transfer at the boundary between a porous medium and a homogeneous fluid. – I. Theoretical development. International Journal of Heat and Mass Transfer 38, 2635–2646.

Ochoa-Tapia, J.A., Whitaker, S., 1995b. Momentum transfer at the boundary between a porous medium and a homogeneous fluid – II. Comparison with experiment. International Journal of Heat and Mass Transfer 38 (14), 2647–2655.

Ouriemi, M., Vasseur, P., Bahloul, A., 2005. Natural convection of a binary fluid in a slightly inclined shallow cavity. Numerical Heat Transfer, Part A (Applications) 48, 547–565.

Patankar, S., 1980. Numerical Heat Transfer and Fluid Flow. Hemisphere, Washington, DC.

Platten, J.K., Legros, J.C., 1984. Convection in Liquids. Springer-Verlag, New York.

Poulikakos, D., Bejan, A., Selimos, B., Blake, K.R., 1986. High Rayleigh number convection in a fluid overlying a porous bed. International Journal of Heat and Fluid Flow 7, 109–114.

Prud'homme, M., Hung Nguyen, T., 2002. Parallel flow stability under a uniform heat flux: effect of the Prandtl number. International Communications in Heat and Mass Transfer 29, 749–756.

Saghir, Z., Comi, P., Mehrvar, M., 2002. Effects of interaction between Rayleigh and Marangoni convection in superposed fluid and porous layers. International Journal of Thermal Sciences 41, 207–215.

Saghir, Z., Jiang, G., Derawi, O., Stenby, H., Kawaji, M., 2004. Theoretical and experimental comparison of the Soret coefficient for water–methanol and water–ethanol binary mixtures. The European Physical Journal E 15, 241.

Shivakumara, S., Suma, S.P., Chavaraddi, B.K., 2006. Onset of surface-tension-driven convection in superposed layers of fluid and saturated porous medium. Archives of Mechanics 58, 71–92.

Somerton, C.W., Catton, I., 1982. On the thermal instability of superposed porous and fluid layers. ASME Journal of Heat Transfer 104, 160–165.

Sparrow, E.M., Goldstein, R.J., Jonsson, V.K., 1964. Thermal instability in horizontal fluid layer – Effect of boundary conditions and non-linear temperature profile. Journal of Fluid Mechanics 18, 513–528.

Turner, J., 1985. Multi-component convection. Annual Review of Fluid Mechanics 17, 11–44.

Vasseur, P., Wang, C.H., Sen, M., 1989. Thermal instability and natural convection in a fluid layer over a porous substrate. Warme und Stoffubertragung 24, 337–347.